Research Article

Muhammad Hasnain Jameel, Shahroz Saleem, Muhammad Hashim, Muhammad Sufi Roslan, Hamoud Hassan Naji Somaily, Mahmoud M. Hessin, Zeinhom M. El-Bahy, Muhammad Gul Bahr Ashiq, Maytham Qabel Hamzah, Abdullah Hasan Jabbar, Jibrin Alhaji Yabagi, and Mohd Arif Bin Agam*

A comparative study on characterizations and synthesis of pure lead sulfide (PbS) and Ag-doped PbS for photovoltaic applications

https://doi.org/10.1515/ntrev-2021-0100 received July 24, 2021; accepted September 25, 2021

Abstract: In this study, a hydrothermal technique was used to synthesize lead sulfide (PbS) and silver (Ag)-doped PbS nanoparticles (NPs) at different concentrations of 20, 40, and 60% of Ag. The small lattice phase changes appeared due to the shifting of diffraction angle peaks toward higher 2θ for samples doped with PbS with increasing Ag content. The analysis of average crystallite size, phase structure, and lattice constant was observed under X-ray diffraction. The value of crystallite size,

Shahroz Saleem, Muhammad Hashim: Department of Physics, University of Agriculture Faisalabad, 38040 Faisalabad, Pakistan Muhammad Sufi Roslan, Maytham Qabel Hamzah: Department of Physics and Chemistry, University Tun Hussein Onn Malaysia, 84600 Muar, Johor, Malaysia

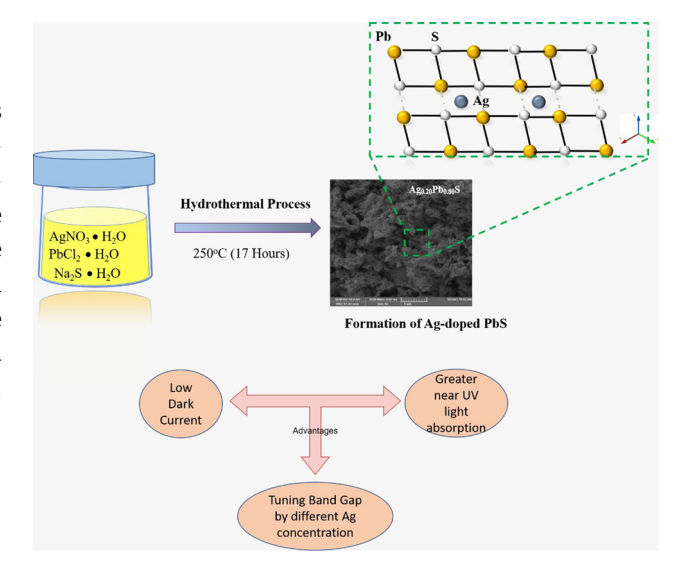
Hamoud Hassan Naji Somaily: Department of Physics, Faculty of Science, King Khalid University, P.O. Box 9004, Abha, Saudi Arabia Mahmoud M. Hessin: Department of Chemistry, College of Science, Taif University, P.O. Box 11099, Taif 21974, Saudi Arabia

Zeinhom M. El-Bahy: Department of Chemistry, Faculty of Science, Al-Azhar University, Nasr City 11884, Cairo, Egypt

Muhammad Gul Bahr Ashiq: Department of Physics, College of Science, Imam Abdulrahman Bin Faisal University, P.O. Box 1982, 31141 Dammam, Saudi Arabia; Basic and Applied Scientific Research Center, Imam Abdulrahman Bin Faisal University, P.O. Box 1982, 31141 Dammam, Saudi Arabia

Abdullah Hasan Jabbar: Optical Department, College of Health and Medical Technology, Sawa University, Ministry of Higher Education and Scientific Research, Al-Muthana, Samawah, Iraq

Jibrin Alhaji Yabagi: Departments of Physics, Faculty of Natural Sciences, Ibrahim Badamasi Babangida University Lapai, P.M.B 11, Lapai, Niger State, Nigeria



Graphical abstract

volume of the unit cell, and porosity (%) were found to increase with the increasing concentration of Ag NPs in PbS. The pure PbS crystallite size is small compared to Ag-doped PbS. The optical characteristics including absorption spectra of the prepared samples were investigated and confirmed by using scanning electron microscope and UV-Vis spectroscopy. The observation of the composition showed that higher doping concentrations of Ag lead to an increase in particle size. Absorption peaks in the UV-Vis spectra corresponding to pure and 20, 40, and 60% of Ag/PbS were observed at different wavelengths of 368, 369, 371, and 372 nm, respectively. Fourier transformation infrared spectroscopy peaks were found in the vibration mode of the ions due to the increment in Ag doping concentrations. These results indicate the possibility of tuning the optical structural properties of Ag-doped PbS through doping various concentrations of Ag NPs. Ag-doped PbS is considered promising future semiconductor nanomaterial, which will enhance the efficiency of photovoltaic device applications.

^{*} Corresponding author: Mohd Arif Bin Agam, Department of Physics and Chemistry, University Tun Hussein Onn Malaysia, 84600 Muar, Johor, Malaysia, e-mail: arif@uthm.edu.my Muhammad Hasnain Jameel: Shaanxy Key Laboratory for Theoretical Physics Frontiers, Institute of Modern Physics, Northwest University, Xi'an 710069, China

[@] Open Access. © 2021 Muhammad Hasnain Jameel *et al.*, published by De Gruyter. © This work is licensed under the Creative Commons Attribution 4.0 International License.

Keywords: Ag/PbS, pure lead sulfide, photovoltaic applications

1 Introduction

Due to its promising and remarkable optoelectronic properties, Ag-doped lead sulfide (PbS) has traditionally been regarded a potential photovoltaic material. Ag-doped PbS has recently received a lot of interest due to its numerous potential applications in modern communication technologies such as global positioning systems, software radio systems, and environmental monitoring satellites. Furthermore, Ag-doped PbS cubic crystalline is used for optical and photonic switching. It is one of the most attractive metal sulfides for a wide range of applications such as Pb²⁺ ion selector sensors and photovoltaic cells [1,2].

In addition, Ag-doped PbS is an important inorganic compound which has been studied for its numerous applications. Ag-doped PbS belongs to II-VI compound semiconductor nano-materials with a cubic crystal structure. The Ag-doped PbS belongs to the space group Fm3m and has the lattice constant $a = 5.939 \,\text{Å}$. The lead and sulfur ions occupy sites 4(a) with coordinates (0, 0, 0) and sites 4(b) with coordinates (1/2, 1/2, 1/2), respectively. Ag-doped lead sulfide (Ag:PbS) seems to be a promising semiconductor material due to its smallest band gap (0.41 eV at 300 K) and large excitation Bohr radius of 18 nm [3,4].

The semiconductor Ag:PbS has photovoltaic and thermoelectric properties [5]. Ag:PbS semiconductor materials have good potential not only due to their tunable optical and electrical characteristics but due to their potential for use in many technological innovations such as solar cells, IR detector, photoconductor photovoltaic cells, and electrochemical storage devices [6,7]. Their properties are dependent on the structure, shape, phase, chemical composition, size, size distribution, and synthesis method of nanoparticles (NPs) [8,9].

Ag:PbS is one of those nanomaterials used by industries for photo-detector and photovoltaic solar cells energy storage applications. The binary compound semiconductor of groups II and IV is prominent nanomaterial to produce photonic devices such as photoconductive cells, solar cells, photocatalytics, LEDs, and memory storage devices. Ag:PbS is a prominent narrow band gap nanomaterial. It is one of the fascinating metal sulfides for a wide range of photo-detector applications [10,11].

Recently Ag:PbS nanostructures have been extensively used for photovoltaic applications. Ag:PbS NP photo-detector shows excellent efficiency [12]. Normally, high dark current lead to high short noise, the noise that occurs due to the low presence of light in the photodetector. Studies show that black crystal of controlled layer phosphorus can be used for optimizing band gap of highly responsive photo-detector at specific wavelength where low dark current certainly achieved [13]. Blocking layers have also been reported to reduce the dark current in tin (II) phthalocyanine in photovoltaic cells [14]. Morphological and molecular structures are also a main factor influencing dark current density in organic photovoltaic devices based on interaction with molecular donor materials [15]. Meanwhile, minimizing dark current had shown a significant effect in speeding up the response of photovoltaic UV detectors [16]. For ensuring the excellent performance of photovoltaic devices dark currents should be less and the dissociation of light generated charge carriers must be enhanced [17]. Ag is a good metal element with unique characteristics. Furthermore, it behaves as an electron contributor when it is substituted into the PbS NPs as a result of decrement in the p-type character, and in turn, the dark currents decrease [18].

In this study, Ag:PbS nanomaterials were found to be convenient and efficient semiconductors for applications in electronic devices. Doping of Ag with any element may influence its structural, optoelectronic, and photonic properties. Ag nanomaterials have received considerable attention because of its extraordinary role in semiconductors for photovoltaic cells [19-21]. In this work, Ag:PbS NPs in the porous form have been prepared using the facile hydrothermal method for applications in electronic devices while using PbCl2 and AgNO3 as chemical reactants at 250°C.

2 Experimental details

Lead chloride (PbCl₂) and Na₂S used in this process as starting chemicals were of high purity grade, and silver nitrate (AgNO₃) was applied as a dopant for all prepared samples except one. X-ray diffraction (XRD) results were obtained through an X-ray diffractometer using nickelfiltered Cu Ka radiation. Scanning electron microscopic (SEM) images were obtained on an LEO device model 1455VP. Absorption wavelength and band gap were observed using 5000 UV NIR spectrophotometer. The Fourier transformation infrared spectroscopy (FTIR) observed on a Perkin-Elmer GX FTIR was used to obtain 10 cm⁻¹ resolution spectrum in the range of 500–4,000 cm⁻¹.

2.1 Preparation of Ag:PbS NPs

Pure PbCl₂ was taken 100% and dissolved in 50 mL distilled water and stirred for 1 h. This was called solution "A." In another beaker with a volume of 250 mL sodium sulfide (Na₂S) 1.95 g was dissolved in 50 mL distilled water and stirred for 1 h. This was called solution "B." Cetyl trimethyl-ammonium bromide (CTAB) 0.1 g was also mixed in the solution of PbCl₂. These solutions were mixed while being continuously stirred in a beaker for 1 h. The quantity of the material was 100 mL. Around 10 mL of ammonia (NH₃) was added in the mixture of PbCl₂ solution inside the flask. The addition of improper resolution (NH₃) was continued till pH 7 was reached. After this step, the solution of mixture of "A" and "B" was about 150 mL.

A PbCl₂ solution of milky color was obtained. Moreover, green color Na_2S was mixed till its color changed to brown. After this, at room temperature, the prepared milky color solution was stirred for 1 h, so that the homogeneity of the prepared solution can be easily maintained. The same procedure was used in samples S_2 , S_3 , and S_4 for 2 h, respectively. Later, $AgNO_3$ was used as dopant for the other three samples. The concentrations were taken as 20% $AgNO_3$ and 80% $PbCl_2$ for sample S_4 , while the concentration of Na_2S was kept the same in all the

four samples. At the bottom of the beaker grains of milky colors were established. Milky color synthesized NPs were cleaned through distilled water till it became neutral (pH = 7). After the cleaning and filtration process, the ending NPs were put into a china dish. The sample was dehydrated in an oven for 2h at 60°C. This solution was kept in two different size autoclaves and kept in the oven for 17 h at the temperature of 250°C as shown in Figure 1. After the samples cooled down they were centrifuged for 5 min at 600 rev s⁻¹. The water was discharged and the process was repeated. The obtained compound is passed through the sonication process. Furthermore, the paste was kept in the furnace for 17 h. Finally, when it dried, the sample was grinded with the help of mortar and pestle to turn it into powder form. PbS samples prepared in different concentration ratios are presented in Table 1.

3 Results and discussion

3.1 Phase analysis by XRD

XRD was used to observe phase formation and the average crystallite size of pure PbS and Ag substituted PbS. Figure 2 shows the XRD results extracted of pure PbS and Ag:PbS

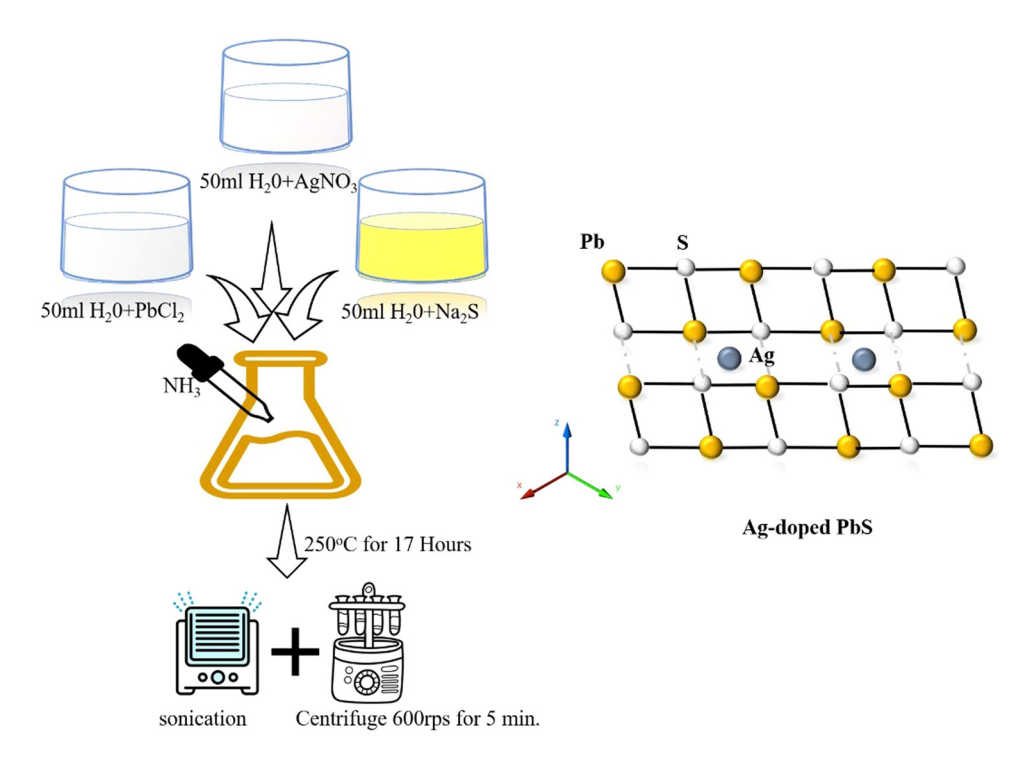


Figure 1: Experimental diagram of sample preparation of pure PbS and Ag:PbS at different concentrations.

Table 1: Samples of PbS (in 50 mL), $AgNO_3$ (in 50 mL), and Na_2S (in 50 mL) prepared with different ratios

Serial no.	PbCl ₂ (g)	AgNO ₃ (g)	Na ₂ S (g)	CTAB (g)	NH ₃ (mL)
Sample S ₁	100%		1.95	0.1	10
Sample S ₂	80%	20%	1.95	0.1	10
Sample S ₃	60%	40%	1.95	0.1	10
$Sample \ S_4$	40%	60%	1.95	0.1	10

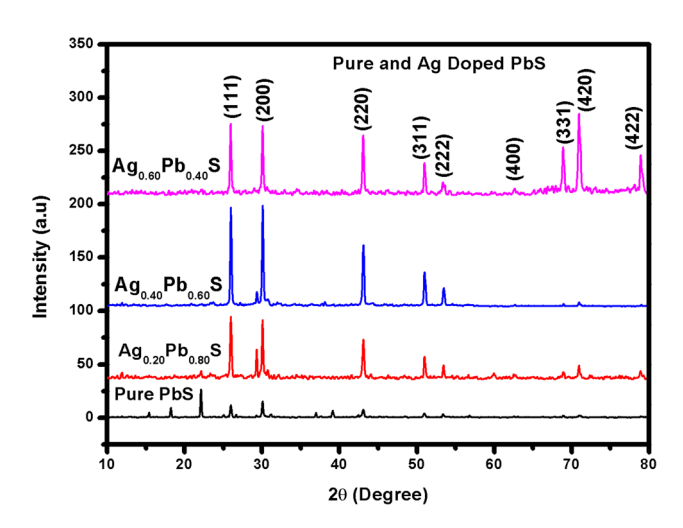


Figure 2: XRD pattern of pure PbS and Ag:PbS at different concentrations: (a) 20%, (b) 40%, and (c) 60%.

NPs at different concentrations of Ag with 20, 40, and 60%. The results showed that the samples had cubic structure and no other impurity was present up to 20%. However, at 60% small impurities were present and at 2θ angle = (50–52.5°), (311) and (222) peaks were not clearly separated. XRD analysis of PbS NPs revealed the formation of cubic phase PbS NPs with the Fm3m space group. It is noted that some peaks were shifted toward higher 2θ while increasing the concentrations of Ag dopant in PbS NPs which may be due to micro strain in the product. As the dopant element Ag was increased from 20, 40, and 60%, the peak for plane (111) was shifted to larger angles, whereas the peak (422) was approximately unchanged. The peaks merged to a single (311) and (331) peak, at a point of 20, 40, and 60% Ag content. Sharp peaks in Figure 2 show that pure PbS NPs have the smallest crystallite size and lattice parameters, but on the other side, the crystalline behavior of Ag:PbS NPs increased with the increase in the concentrations of 20, 40, and 60% of Ag dopant. The findings showed that the cubic structure of Ag:PbS with increasing content of Ag has small distortions.

Lattice constant (a) states the physical quantity of unit cells. Lattice constants in three dimensions mostly have three constants, represented as a, b, and c. Interplanar spacing (h, k, l) are designated planes and prominent miller indices adjacent planes [22].

The crystallite size (D) is a calculation made from XRD investigation referring to certain angles using Scherrer's formula. Crystallite size is calculated in nanometer. The factor (K) in its shape range changes with the original shape of the crystal Θ is signify of Bragg's angle. β is represents the line broadening (bisector) at half intensity of XRD peak, after removing the helpful line increase, in radians (r) [23].

$$D = \frac{K\lambda}{\beta \cos \Theta}.$$
 (1)

Atomic packing factor of cubical architecture can be calculated through the following formula [24–26]:

$$P = \frac{1 \star \frac{4}{3} \pi \left(\frac{1}{2} a\right)^3}{a^3},\tag{2}$$

$$a = d\sqrt{h^2 + l^2 + k^2},\tag{3}$$

$$V = a^3. (4)$$

Density (ρ_x) of X-ray can be observed by using the following formula:

$$\rho_{x} = \frac{ZM}{N_{\Lambda}}, \tag{5}$$

where Z indicates the atomic number contained in a unit cell (Z=8), M denotes the compound molecular weight of, and N_A is the Avogadro number [27].

$$\rho_{x} = \frac{n M_{\text{W}}}{N_{\text{A}} V}.$$
 (6)

Strain of the unit cell of a crystal lattice can be calculated using the following equation [28]:

Strain =
$$\frac{k\lambda}{D}$$
. (7)

The crystallite size of the samples was found to be 6.49 nm for undoped PbS but 7.54, 8.43, and 9.55 nm for 20, 40, and 60% of Ag-doped NP respectively as shown in Table 2. The porosity significantly increases with the increase of Ag-doped NP in sintering temperature as shown in Figure 3 [29–31]. In equation (8) density (ρ_x) of X-ray and (ρB) donates bulk density.

Porosity =
$$\left(1 - \frac{\rho B}{\rho x}\right) \times 100\%$$
. (8)

Table 2: Lattice parameters for pure PbS and Ag:PbS at (a) 20%, (b) 40%, and (c) 60%

Calcination Ag content	Crystallite size (nm)	d-spacing	Lattice constant	X-ray density (g cm ⁻³)	Porosity (%)
Pure	6.49	2.8882	5.7764	1.6489	3.51
20% Ag	7.54	2.9672	5.9344	1.5206	3.65
40% Ag	8.43	2.9695	5.9390	1.5171	5.98
60% Ag	9.55	2.9729	5.9458	1.5119	8.65

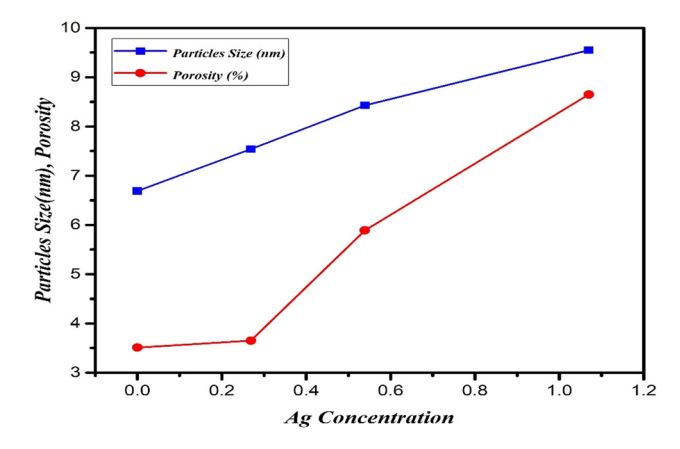


Figure 3: Ag concentration and particles size, porosity of undoped and doped PbS.

3.2 Morphology studied by SEM

SEM was used in the micro-structural analysis of the samples. The specimens were studied for grain size and morphology. The SEM micrograph of pure PbS and Ag:PbS clearly showed in Figure 4 that there was an inhomogeneous distribution of various sizes and morphology. The formation of nano-rods of pure PbS and an agglomeration of NPs of Ag:PbS of various sizes were seen. The formation of the agglomeration of NPs might enhance the usability of Ag:PbS samples. There was a significant change in pure PbS and morphology by the addition of Ag atoms into the PbS. The average grain size as measured from SEM images was 19.48, 21.50, and 27.50 nm for 20, 40, and 60% for Ag:PbS respectively. One concludes from the SEM images

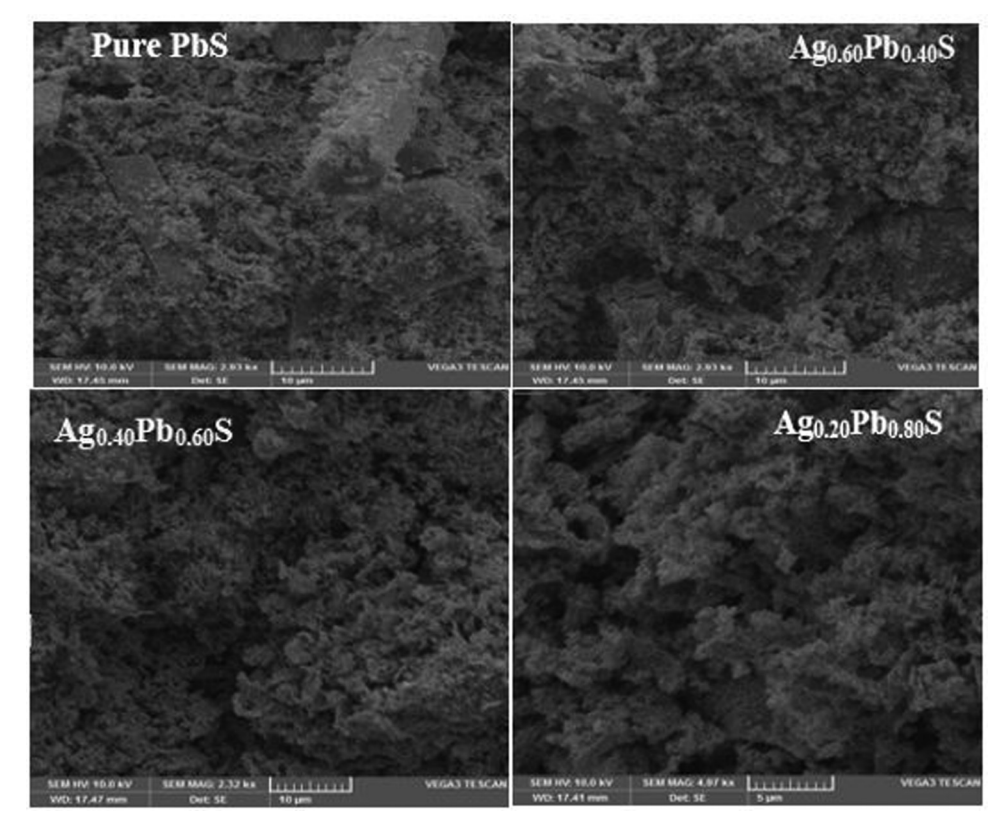


Figure 4: SEM micrographs of pure PbS and Ag:PbS at different concentrations: (a) 20%, (b) 40%, and (c) 60%.

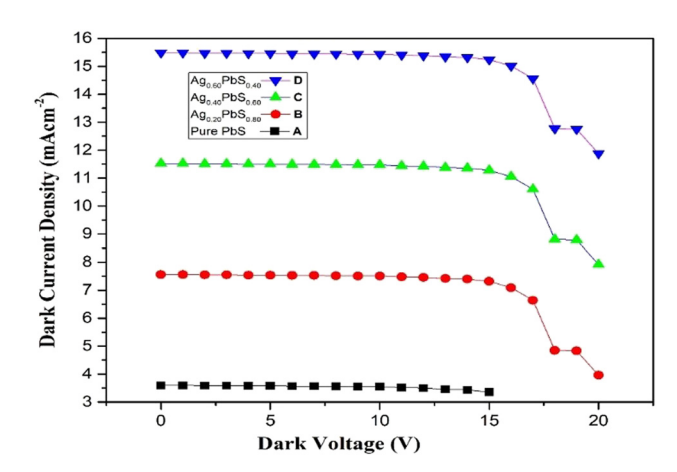


Figure 5: Dark current for pure PbS and Ag:PbS at different concentrations: (a) 20%, (b) 40%, and (c) 60%.

that the particle size increased with the increment of Ag concentration in PbS samples.

3.3 Dark current measurement for pure and Ag:PbS

A dark current diode was used to conduct dark current suppression. Dark current is a small amount of current that flow through photovoltaic devices such as photodiode, solar cells, photoconductor, IR detector, charge-coupled devices, and photovoltaic cells. For the excellent performance of photovoltaic devices dark currents should be less and dissociation of light generated charge carriers must be enhanced. Ag is a good metal element with unique characteristics. Furthermore, it behaves as an electron contributor when it is substituted into the PbS NPs as a result of decrement in p-type character, and in turn, the dark currents decrease as shown in Figure 5.

3.4 UV-Vis and band gap studies

UV-Vis absorption is studied along with the band gap measurements of pure PbS and with 20, 40, and 60% concentration of Ag:PbS as given in Figure 6. The absorption measurement has been carried out in a range of wavelengths between 200 and 900 nm. Absorption characteristic peak at wavelength 368 nm appeared for pure PbS sample. But absorption characteristics peak at wavelengths 369, 371, and 372 nm with 20, 40, and 60% concentration of Ag:PbS, respectively. According to the calculation made from the equation (9), the band gap

value for (c) 60% of Ag:PbS was determined at 5.16 eV. A prominent red shift appeared for Ag-PbS in the absorption spectra compared to the pure PbS sample. UV-Vis absorption spectra measurements indicate that Ag-PbS samples can absorb more light than pure PbS samples.

UV-Vis absorption spectra for (c) 60% g concentration of Ag:PbS is shown in Figure 6s. Using Tauc's equation, the energy band gap of doped samples can be calculated through the tangent line in the plot of $(\alpha h v)^n$ [32–34].

$$(\alpha h v) = k(h v - E_{\rm g})^n, \tag{9}$$

where " α " is absorbance coefficient, "hv" is the incident photon energy, "k" is energy independent constant, and " E_g " is the energy gap of the optical band [34–36]. The band gap value was calculated at 5.16 eV by applying equation (9) for the absorption spectrum at wavelength 372 nm. The band gap measurements for pure PbS and 20, 40, and 60% concentration of Ag:PbS, respectively, is shown in Table 3. It has been clearly found that the Ag-PbS band gap increased as Ag concentration increased as shown in Figure 7. The data of the optical band gap for pure PbS and Ag:PbS are shown in Table 3, where the band gap value is in the range of 4.50-5.16 eV which has become ultra-wide band gap semiconductor material. Generally, wide band gap semiconductors have electronic properties which fall in between conventional semiconductor and insulators. The higher energy gap gives devices the ability to operate at higher temperature and power switching. Furthermore, the bandgap shrinks with increasing temperature. Wide band semiconductors are useful at shorter wavelengths than other semiconductor materials.

3.5 FTIR

The infrared spectrum is an important tool to probe different ordering phenomena. This technique provides information about the position of ions in the crystal, geometry, interaction of molecules, and the crystal vibration modes. The FTIR spectra of pure PbS and Ag:PbS were measured in the range of 500–4,000 cm⁻¹ at different concentrations of 20, 40, and 60% of Ag:PbS, respectively. The FTIR spectra of pure and Ag:PbS possess four characteristic bands in the range of 500–3,000 cm⁻¹. The values of bands according to the wave number of pure PbS are 1,036 and 3,006 cm⁻¹, at 20%-Ag 685, 1,026, 1,382, 2,990 cm⁻¹ and at 40%-Ag bands value are 659, 1,020, 1,372, and 2,990 cm⁻¹. Similarly at 60%-Ag bands value are 649, 1,015, 1,351, and 2,943 cm⁻¹.

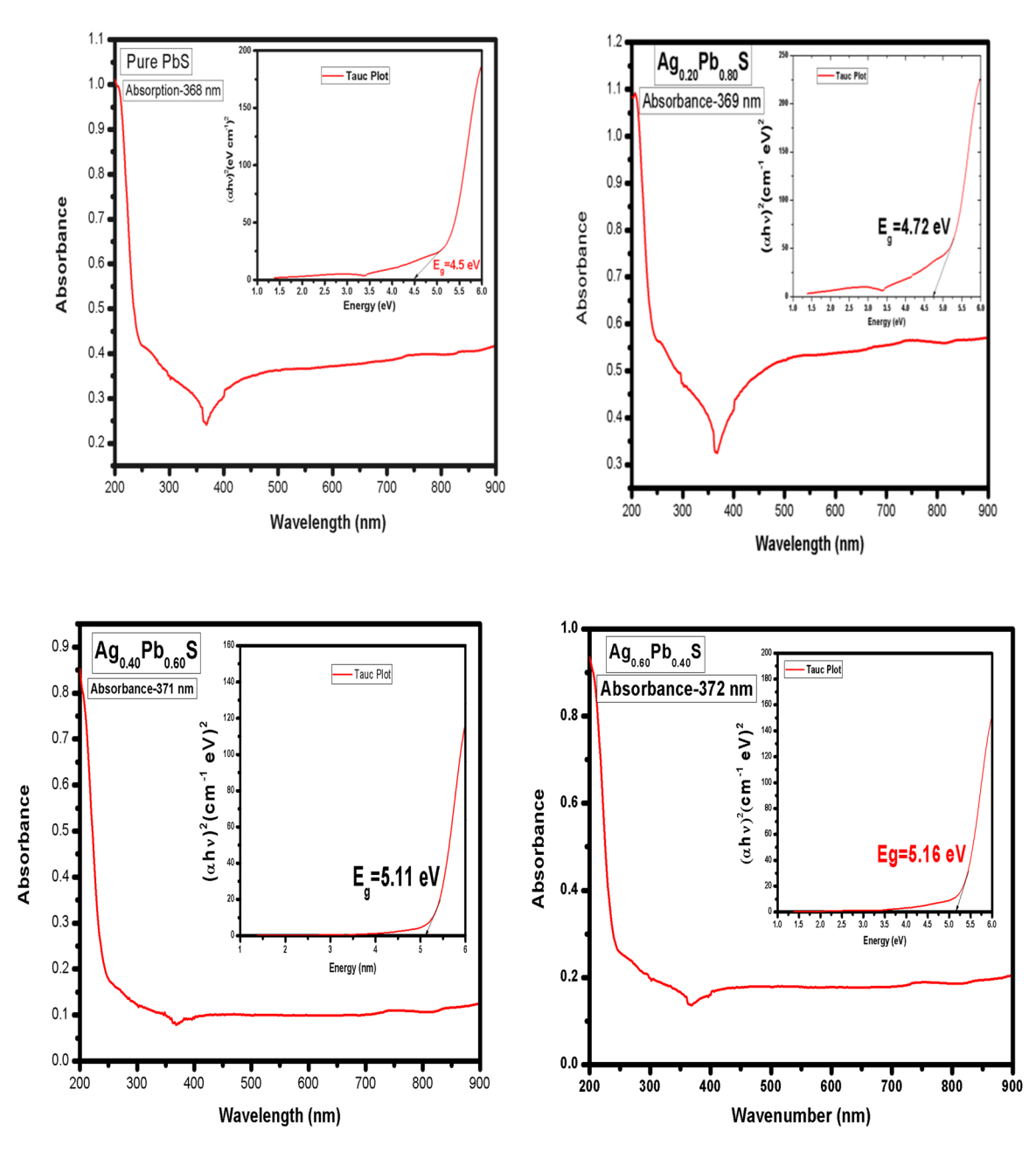


Figure 6: UV-Vis absorption spectra for pure PbS and Ag:PbS at different concentrations: (a) 20%, (b) 40%, and (c) 60%.

Table 3: Band gap for pure PbS and Ag:PbS at (a) 20%, (b) 40%, and (c) 60%

Ag content (g)	Absorption wavelength (nm)	Band gap (eV)
Pure PbS	368	4.50
20%	369	4.72
40%	371	5.11
60%	372	5.16

This band pattern is assigned with the vibration mode of Ag and lead ions due to the increment of Ag concentration. This pattern indicates that band's values are increased by increasing the Ag-doped concentration, which is shown in Figure 8. The value of transmittance is also decreased by Ag-doped concentration. However, the higher frequency band 685 cm⁻¹ is shifted to the lower frequency band 649 cm⁻¹ by increasing Ag doping concentration.

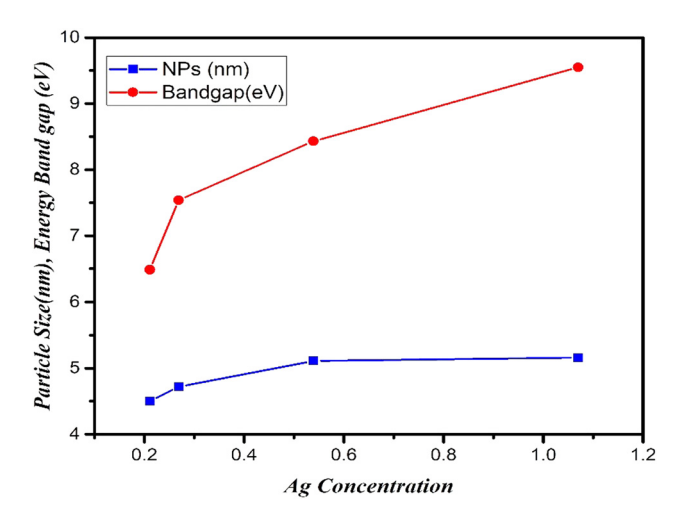


Figure 7: Ag concentration with particles size and band gap energy of pure PbS and Ag:PbS.

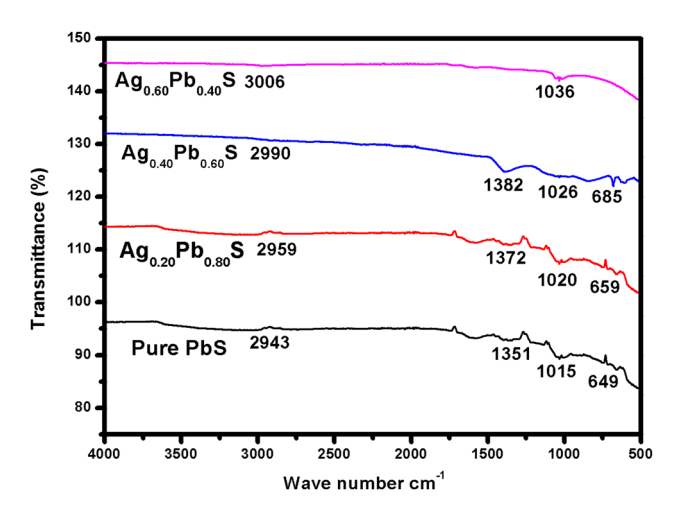


Figure 8: FTIR spectra for pure PbS and Ag:PbS at different concentrations: (a) 20%, (b) 40%, and (c) 60%.

4 Conclusion

In this study, a hydrothermal technique was used to synthesize PbS and Ag"PbS NPs at different concentrations of Ag for photovoltaic device application. The lattice distortion or phase changes appeared due to the shifting of diffraction angle peaks to higher 2θ in the samples of Ag:PbS with increasing Ag content. The values of the crystallite's size, volume of the unit cell, and porosity (%) were found to increase with the increasing concentrations of Ag NPs in PbS. The pure PbS crystallite's size is relatively small compared to Ag:PbS. The dark current decreased presumably because of the decrement in p-type character with the increment in Ag doping into

PbS NPs. Absorption peaks in UV-Vis spectra corresponded to pure, 20, 40, and 60% of Ag:PbS, observed at different wavelengths of 368, 369, 371, and 372 nm, respectively. FTIR peaks found that vibration mode of ions due to increment Ag doping concentration. Experimental results indicate the possibility of tuning the optical structural properties of Ag:PbS through the doping of various concentrations of Ag NPs. Ag:PbS are promising semiconductor nanomaterials that can enhance the efficiency of photovoltaic device applications.

Acknowledgements: This work was funded by the Taif University Researchers supporting Project number (TURSP-2020/109), Taif University, Taif, Saudi Arabia. The authors also extend their appreciation to the Deanship of Scientific Research at the King Khalid University for financial support through the research groups program under grant number (R.G.P. 2/171/42).

Funding information: Taif University Researchers supporting Project number (TURSP-2020/109), Taif University, Taif, Saudi Arabia. The authors also extend their appreciation to the Deanship of Scientific Research at the King Khalid University for financial support through the research groups program under grant number (R.G.P. 2/171/42).

Author contributions: All authors have accepted responsibility for the entire content of this manuscript and approved its submission.

Conflict of interest: The authors state no conflict of interest.

References

- Lifshitz E, Sirota M, Porteanu H. Synthesis and characterization of nickel doped cadmium sulfide (CdS: Ni²⁺) nanoparticles. Mater Res Bull. 1999;196:126–34.
- [2] Zhao Y, Liao X, Hong J, Zhu J. Synthesis of lead sulfide nanocrystals via microwave and sonochemical methods. Mater Chem Phys. 2004;87:149-53.
- [3] Giribabu K, Suresh R, Manigandan R, Vijayalakshmi L. Hydrothermal synthesis of lead sulphide nanoparticles and their electrochemical sensing property. Adv Mater Res. 2012;584:276–9.
- [4] Duan T, Lou W, Wang X, Xue Q. Size-controlled synthesis of orderly organized cube-shaped lead sulfide nanocrystals via a solvothermal single-source precursor method. Colloids Surf A Physicochem Eng Asp. 2007;310:86-93.
- [5] Yang YJ. A novel electrochemical preparation of PbS nanoparticles. Mater Sci Eng B. 2006;131(1-3):200-2.
- [6] Phuruangrat A, Thongtem S, Kuntalue B. Sonochemical synthesis and characterization of lead sulfide nanoparticles. Dig J Nanomat Biostruct. 2012;7(4):1413–7.

- [7] Chongad LS, Sharma A, Banerjee M, Jain A. Synthesis of lead sulfide nanoparticles by chemical precipitation method. J Physics Conf Ser. 2016;755:012032.
- [8] Arif M, Jameel MH, Hamzah MQ, Ruslan MS, Rizvi SZH. Coprecipitation method in synthesis and characterization of BiFeO₃ doped with various concentrations of Mn nanoparticles for electronic device applications. Test Eng Mannag. 2020:83:22302-9.
- [9] Ali A, Uddin S, Iqbal Z, Lal M, Jameel MH, Zaman A, et al. Synthesis and characterizations of $(Ba_{1-x}Ca_x)$ Ti_4O_9 , $0 \le x \le 0.9$ ceramics. J Mater Res Technol. 2021;11:2-7.
- [10] Jameel MH, Hamzah MQ, Arif M, Agam B. Synthesis and characterizations of Co-doped TiO2 nanoparticles via coprecipitation method. Solid State Technol. September, 2020;63(1):267-77.
- [11] Kuljanin J, Comor MI, Djokovi V, Nedeljkovi JM. Synthesis and characterization of nanocomposite of polyvinyl alcohol and lead sulfide nanoparticles. Mater Chem Phys. 2006;95:67-71.
- [12] Pourmortazavi SM, Hajimirsadeghi SS. Statistical optimization of condition for synthesis lead sulfide nanoparticles statistical optimization of condition for synthesis. Mater Manuf Process. 2009;6914:524-8.
- [13] Youngblood N, Chen C, Koester SJ, Li M. Waveguide-integrated black phosphorus photodetector with high responsivity and low dark current. Nat Photonics. 2015;9(4):247-52.
- [14] Li N, Lassiter BE, Lunt RR, Wei G, Forrest SR. Open circuit voltage enhancement due to reduced dark current in small molecule photovoltaic cells. Appl Phys Lett. 2009;94(2):13.
- [15] Perez MD, Borek C, Forrest SR, Thompson ME. Molecular and morphological influences on the open circuit voltages of organic photovoltaic devices. J Am Chem Soc. 2009;131(26):9281-6.
- [16] Liu Z, Zhao D, Min T, Wang J, Chen G, Wang H-X. Photovoltaic three-dimensional diamond UV photodetector with low dark current and fast response speed fabricated by bottom-up method. IEEE Electron Device Lett. 2019;40(7):1186-9.
- [17] Ghanbari D, Salavati-niasari M, Davar F. Synthesis of different morphologies of PbS nanostructures via hydrothermal process. High Temp Mater Process. 2012;31(6):707-10.
- [18] Reisfeld R. Nanosized semiconductor particles in glasses prepared by the sol-gel method: their optical properties and potential uses. J Alloy Compd. 2002;341:56-61.
- [19] Scanning FE. The effect of capping agent on the structural, optical properties and photocatalytic activity of MgO nanostructures. Phys B: Phys Condens Matter. 2020;583:1-7.
- [20] Karami H, Ghasemi M, Matini S. Synthesis, characterization and application of lead sulfide nanostructures as ammonia gas sensing agent. Int J Electrochem Sci. 2013;8:11661-79.
- [21] Manouchehri S, Zahmatkesh J, Yousefi MH. Substrate effects on the structural properties of thin films of lead sulfide. J Optoelectron Nanostruct. 2018;3(2):1-18.
- [22] Sadovnikov SI, Kozhevnikova NS, Rempel AA. The structure and optical properties of nanocrytalline lead sulfide films. Semiconductors. 2010;44(10):1349-56.
- [23] Sadovnikov SI, Ishchenko AV, Weinstein IA. Synthesis and optical properties of nanostructured ZnS and

- heteronanostructures based on zinc and silver sul fi des. J Alloy Compd. 2020;831:154846.
- [24] Saraidarov T, Reisfeld R. Synthesis and characterization of lead sulfide nanoparticles in zirconia-silica-urethane thin films prepared by the Sol-Gel process. J Sol-gel Sci Technol. 2003;26:533-40.
- [25] Shkir M, Khan MT, Ashraf IM, AlFaify S, EL-Toni AM, Aldalbahi A. et al. Rapid microwave-assisted synthesis of Agdoped PbS nanoparticles for optoelectronic applications. Ceram Int. 2019;45(17):21975-85.
- [26] Offor PO, Whyte GM, Ezekoye VA, Omah AD, Ode SN, Ocheri C, et al. Structural, morphological and optical properties of sprayformed silver-doped zinc sulphide thin films. Opt Int J Light Electron Opt. 2019:185:519-28.
- [27] Truong L, Moody IS, Stankus DP, Je V, Mark AN, Tanguay RL. Differential stability of lead sulfide nanoparticles in influences biological responses in embryonic zebrafish. Archive Taxicol. 2011;85(7):787-98.
- [28] Nanoparticles S, Ali MM, Mahdi HS, Parveen A, Azam A. Microstructural and optical properties of silver doped cadmium sciencedirect microstructural and optical properties of silver doped cadmium sulphide nanoparticles. Mater Today Proc. 2019;18:717-22.
- [29] Elango M, Nataraj D, Nazeer KP, Thamilselvan M. Synthesis and characterization of nickel doped cadmium sulfide (CdS: Ni2 +) nanoparticles. Mater Res Bull. 2012;47(6):1533-8.
- [30] Durán-toro VM, Price RE, Maas M, Brombach CC, Pichler T, Rezwan K, et al. Amorphous arsenic sulfide nanoparticles in a shallow water hydrothermal system. Mar Chem. 2019;211:25-36.
- [31] Emadi H, Salavati-niasari M. Superlattices and microstructures hydrothermal synthesis and characterization of lead sulfide nanocubes through simple hydrothermal method in the presence of [bis (salicylate) lead (II)] as a new precursor. Superlatt Microstruct. 2013;54:118-27.
- [32] Jyothilakshmi VP, Bhabhina NM, Dharsana MV, Swaminathan S. Materials Today: Proceedings Wet chemical synthesis of lead sulfide nanoparticles and its application as light harvester in photovoltaic cell. Mater Today Proc. 2020:33(3):2125-9.
- [33] Jadhav UM, Patel SN, Patil RS. Synthesis of silver sulphide nanoparticles by modified chemical route for solar cell applications. Res J Chem Sci. 2013;3(7):69-74.
- [34] Yanuar H, Iwantono B, Nabok AV. Short communication formation and UV-Vis studies of lead sulfide nanoparticles. J Nano Electron Phys. 2019;11(2):1-4.
- [35] Pirgholi G, Farjami S, Kalandaragh YA. The influence of irradiation intensity and stirring rate on the photocatalytic activity of titanium dioxide nanostructures prepared by the microwave-assisted method for photodegradation of MB from water. Phys B Phys Condens Matter. January 2020;578:411886.
- [36] Hosseini Z, Kalandaragh YA, Khudayari A, Shakarab BN. Sonochemically prepared PbS nanostructures and investigation of their optical and structural properties. Optoelectron Adv Mater Rapid Commun. 2014;8:201-3.